Toward panchromatic organic functional molecules: Density functional theory study on the nature of the broad UV–Vis–NIR spectra of substituted tetra(azulene)porphyrins

Dongdong Qi, Lijuan Zhang, Jianzhuang Jiang*

Beijing Key Laboratory for Science and Application of Functional Molecular and Crystalline Materials, Department of Chemistry, University of Science and Technology Beijing, Beijing 100083, China

ABSTRACT

To achieve full solar spectrum absorption of organic dyes for organic solar cells and organic solar antenna collectors, a series of tetra(azulene)porphyrin derivatives including $H_2(TAzP)$, $H_2(\alpha$-$F_4TAzP)$, $H_2(\beta$-$F_4TAzP)$, $H_2(\gamma$-$F_4TAzP)$, $H_2(\delta$-$F_4TAzP)$, $H_2(\varepsilon$-$F_4TAzP)$, $H_2(\zeta$-$F_4TAzP)$, $H_2[\alpha$-$(NH_2)_4TAzP]$, $H_2[\beta$-$(NH_2)_4TAzP]$, $H_2[\gamma$-$(NH_2)_4TAzP]$, $H_2[\delta$-$(NH_2)_4TAzP]$, $H_2[\varepsilon$-$(NH_2)_4TAzP]$, and $H_2[\zeta$-$(NH_2)_4TAzP]$ were designed and their electronic absorption spectra were systematically studied on the basis of TDDFT calculations. The nature of the broad and intense electronic absorptions of $H_2(TAzP)$ in the range of 500–1450 nm is clearly revealed. In addition, different types of $\pi \rightarrow \pi^*$ electronic transitions associated with different absorption bands are revealed to correspond to different electron density moving direction between peripherally-fused ten electron-π-conjugated azulene units and the central eighteen electron-π-conjugated porphyrin core. Introduction of electron-donating groups onto the periphery of $H_2(TAzP)$ macrocycle is revealed to be able to lead to novel NIR dyes such as $H_2[\alpha$-$(NH_2)_4TAzP]$ and $H_2[\varepsilon$-$(NH_2)_4TAzP]$ with regulated UV–Vis–NIR absorption bands covering the full solar spectrum in the range of 300–2500 nm. In addition, the basic designing rules for panchromatic organic functional molecules based on tetrapyrrole derivatives are proposed together with the suggestions in experiments, including low molecular symmetry and narrow gap between HOMO and LUMO/LUMO+1, which will be helpful toward the design and synthesis of new panchromatic organic functional molecules.

1. Introduction

Near infra-red (NIR) dyes have received considerable attentions in recent years due to their potential applications in solar cells [1–7], photodynamic therapy for cancer [8–11], NIR imaging [12–15], solar antenna collectors [16–18], and astronomical telescopes [19,20]. Tetrapyrrole derivatives, in particular porphyrins, phthalocyanines, and naphthalocyanines, are among the most important functional molecular materials with intense NIR absorption due to their high photo-chemical stability and intense absorption in the NIR region [21–28]. In recent years, a new skeleton of tetrapyrrole derivatives, tetra(azulene)porphyrins (TAzPs), with significantly intensified NIR absorption in the range of 900–1300 nm was synthesized [29,30]. Nevertheless, the very intense absorptions covering an astonishing broad UV, visible, and NIR range from 300 to 1400 nm revealed in their electronic absorption spectra suggest their great potentials in the fields of organic solar antenna collectors and organic solar cells [29–34].

Investigations in inorganic solar antenna collectors have made significant progress [35]. Actually multilayered inorganic solar antenna collector with absorption ability as high as nearly 90% of the full solar energy was reported [36]. In addition, solar cell fabricated from inorganic semiconductors can also reach high photo-electron transition efficiency of ∼75% due to their intense absorptions over the full UV–Vis–NIR region of solar spectrum [37]. However, exploration in molecular functional materials with application in organic solar antenna collectors [38,39] and/or organic solar cells [35] appears to still be limited to those with absorptions in the UV–Vis region without extending into the NIR region. Taking account of the quite high ratio of NIR region emission over the total solar energy [26], 43%, easily synthesized and stable organic NIR dyes become highly desired towards high efficiency solar antenna collectors and solar cells [31–34].

Recently, an inorganic band-anticrossing full solar spectrum absorption material GaN_xAs_{1-x} was prepared by López and co-workers [40]. By inserting an intermediate energy band between the former valence band (VB) and conduction band (CB), the

absorptions in the UV and visible range of the intrinsic material was extended into the NIR region due to the resulting narrow gaps [40]. In a similar manner, in the case that more extraneous orbitals are inserted into the original frontier orbitals of specific organic dyes with conjugated molecular structure, novel dyes with absorption extending into the NIR region are also expected to improve the efficiency of organic solar antenna collectors and solar cells [26].

Concerning the tetra(azulene)porphyrin (TAzP), significant interaction can be expected to exist between the central eighteen electron-π-conjugated porphyrin core and the four peripherally-fused ten electron-π-conjugated azulene units in the TAzP skeleton, leading to densely-distributed frontier orbitals and narrower gaps between these orbitals. This in turn will induce remarkably red-shifted broad Q bands into the NIR region, resulting in complicated electron absorption spectrum of tetra(azulene)porphyrins (TAzPs) relative to most general porphyrins (Pors) [41–43], tetraazaporphyrins (TAPs) [43], phthalocyanines (Pcs) [43–46], naphthalocyanines (Ncs) [47,48], and even many core-modified porphyrins [49–57]. In addition, the absorption spectra of some sandwich-type multi(tetarpyrrole) metal multiple-decker complexes can also cover such a broad NIR region [58–65]. However, their absorption intensity in this region is much weaker than TAzPs. Nevertheless, Osuka and co-workers synthesized a series of fully conjugated porphyrin tapes and porphyrin arrays also with broad and intense NIR electronic absorptions in their spectra, which significantly increases their light harvesting ability [1–3]. However, the great difficulty in their large scale of preparation precludes their wide range of applications in corresponding field. In good contrast, with a limited macrocyclic tetrapyrrole molecular skeleton, the preparation of TAzPs is relatively easy in terms of large scale synthesis in comparison with either the sandwich-type multi(tetarpyrrole) metal multiple-decker complexes or the conjugated porphyrin tapes, therefore revealing their great potential as organic NIR dyes.

In the present paper, the electronic structures and electronic absorption spectra of a series of H_2(TAzP) have been theoretically investigated on the basis of density functional theory (DFT) and time dependent density functional theory (TDDFT) calculations. Introduction of electron-withdrawing or electron-donating groups onto the periphery of TAzP skeleton further tunes the HOMO–LUMO gap, inducing obvious red/blue-shift of the NIR electronic absorption bands of $H_2[\alpha\text{-}(NH_2)_4TAzP]/H_2[\varepsilon\text{-}(NH_2)_4TAnP]$ into the range of 1000–2500 nm. Moreover, in combination with the previous results [22,25–30,58–65], general rule regarding the design of panchromatic organic functional molecules is also proposed.

2. Computational summary and validity

Hybrid generalized gradient approximation (hGGA) method B3LYP [66,67] is proved suitable for the geometry optimization of porphyrins, phthalocyanines, as well as their various analogs [68–72]. As a consequence, in the present study B3LYP functional was employed for conducting the geometry optimization of the series of TAzP derivatives, Scheme 1. However, B3LYP always overestimates the transition energies for this type of large conjugated system, while generalized gradient approximation (GGA) method significantly improves the agreement between theoretical and experimental results [26,27,73–77]. As a result, GGA functional BP86 [78,79] with Becke88 exchange functional and Perdew86 correlation functional was used to simulate the photon-induced transition densities [26]. In order to further verify the reliability of our TDDFT computation results, the comparison between the calculated and experimental electronic absorption spectrum of tetra(azulene)porphyrins [H_2(TAzP)] was shown in Supporting Information.

In addition, Pople basis sets have been proved excellent for calculating the structure and properties of porphyrins and phthalocyanines as well as their analogs [80–83], leading to many applications in this field. Both DFT and TDDFT calculations were carried out using the basis set of 6-311++G(d,p). In addition, reduced density gradient (RDG) [84–86] and localized orbital locator (LOL) [85–90] were all calculated to explain corresponding properties. All the calculations are carried out using Gaussian 03 [91] and Multiwfn 2.1 [85,86]. Computational details are listed in Supporting Information.

3. Results and discussion

As shown in Scheme 1 and Table S1 (Supporting Information), direct fusion between the porphyrin (central core) and azulene (peripheral substituents) leads to tetra(azulene)porphyrins [H_2(TAzP)] with extended conjugated molecular skeleton. There are six types of substituent sites α, β, γ, δ, ε, and ζ in this porphyrin molecule. NH_2 and F are chosen as the representative electron-donating and -withdrawing groups, respectively [25,26,92–97], leading to a series of tetra(azulene)porphyrin derivatives including H_2(TAzP), $H_2(\alpha\text{-}F_4TAzP)$, $H_2(\beta\text{-}F_4TAzP)$, $H_2(\gamma\text{-}F_4TAzP)$, $H_2(\delta\text{-}F_4TAzP)$, $H_2(\varepsilon\text{-}F_4TAzP)$, $H_2(\zeta\text{-}F_4TAzP)$, $H_2[\alpha\text{-}(NH_2)_4TAzP]$, $H_2[\beta\text{-}(NH_2)_4TAzP]$, $H_2[\gamma\text{-}(NH_2)_4TAzP]$, $H_2[\delta\text{-}(NH_2)_4TAzP]$, $H_2[\varepsilon\text{-}(NH_2)_4TAzP]$, and $H_2[\zeta\text{-}(NH_2)_4TAzP]$.

3.1. Molecular structure and electronic structure

Fig. 1a and Table S1 (Supporting Information) show the optimized molecular structure of metal-free tetra(azulene)porphyrin [H_2(TAzP)] together with a scheme indicating that fusion between the four peripheral ten electron-π-conjugated azulene units (π^{Az}_{10e} units) and a central eighteen electron-π-conjugated porphyrin core (π^{Por}_{18e} core) forms the tetra(azulene)porphyrin skeleton. Fig. 1b shows the localized orbital locator (LOL) of all the π orbitals of the TAnP skeleton. In the LOL scheme, the π electron density is significantly localized between the anthracene and porphyrin units, confirming that fusing the central π^{Por}_{18e} core with four π^{Az}_{10e} units leads to the uniform non-coplanar conjugated system π^{TAzP}_{58e} in the TAzP skeleton. In comparison with the azulene ten-electron conjugated system and porphyrin eighteen-electron conjugated system, this type of tetra(azulene)porphyrin with fifty-eight-electron conjugated system provides much more densely-distributed coupled frontier orbitals, which in turn results in many narrow gaps between frontier molecular orbitals [29,30]. This actually just resembles the inorganic full solar spectrum absorption material GaN_xAs_{1-x} reported recently as mentioned above [40]. Briefly summarizing above, bond interaction analysis for TAzP skeleton shows that fusion of the central π^{Por}_{18e} core and four π^{Az}_{10e} units forms the conjugated system in the TAzP skeleton and results in the densely-distributed TAnP frontier orbitals.

The non-bond interaction analysis of TAnP is shown in Fig. 2 and Fig. S1 (Supporting Information). Obviously, due to the steric hindrance of the peripheral azulene units as well as the α-H atoms, H_2(TAzP) employs a saddle structure instead of the planar one as for metal free porphyrin [H_2(Por)] and azulene (Az), therefore leading to a distorted π^{TAzP}_{58e} system. It is worth pointing out that the balance between the repulsive force (between the α-H atoms of the peripheral azulene units) and the π^{TAzP}_{58e} planar tendency induces the saddle H_2(TAzP) structure. As for TAzPs, the distorted TAzP skeleton is maintained since the peripheral substituents do have little influence on the molecular distorting degree, Table S1 (Supporting Information).
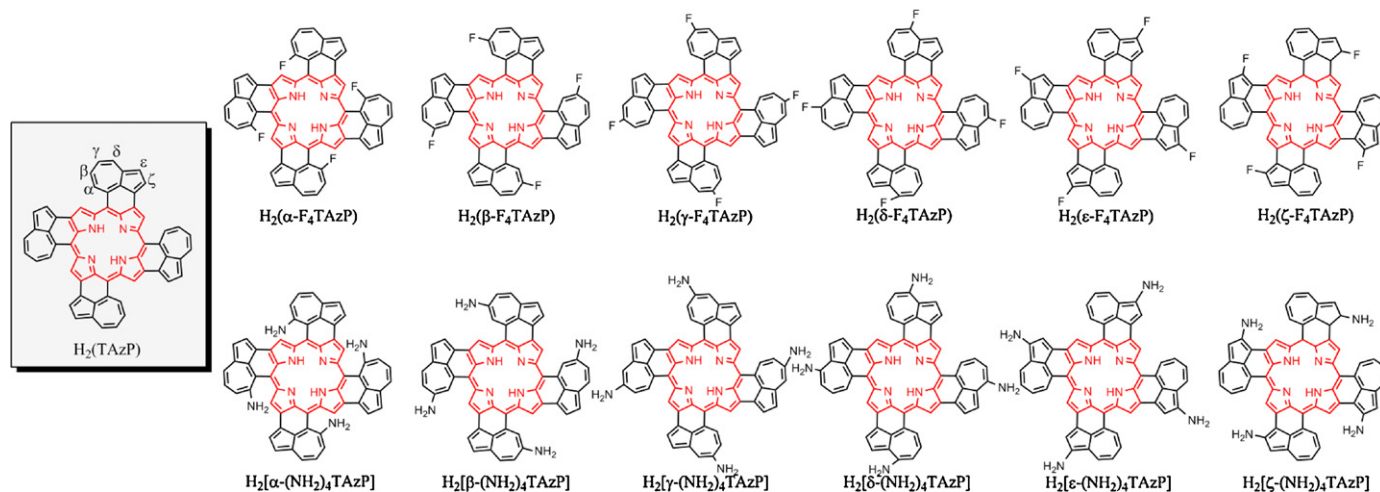
Scheme 1. Molecular structures of $H_2(TAzP)$ and its derivatives with peripheral electron-donating/-withdrawing groups (NH_2 and F as the representatives).
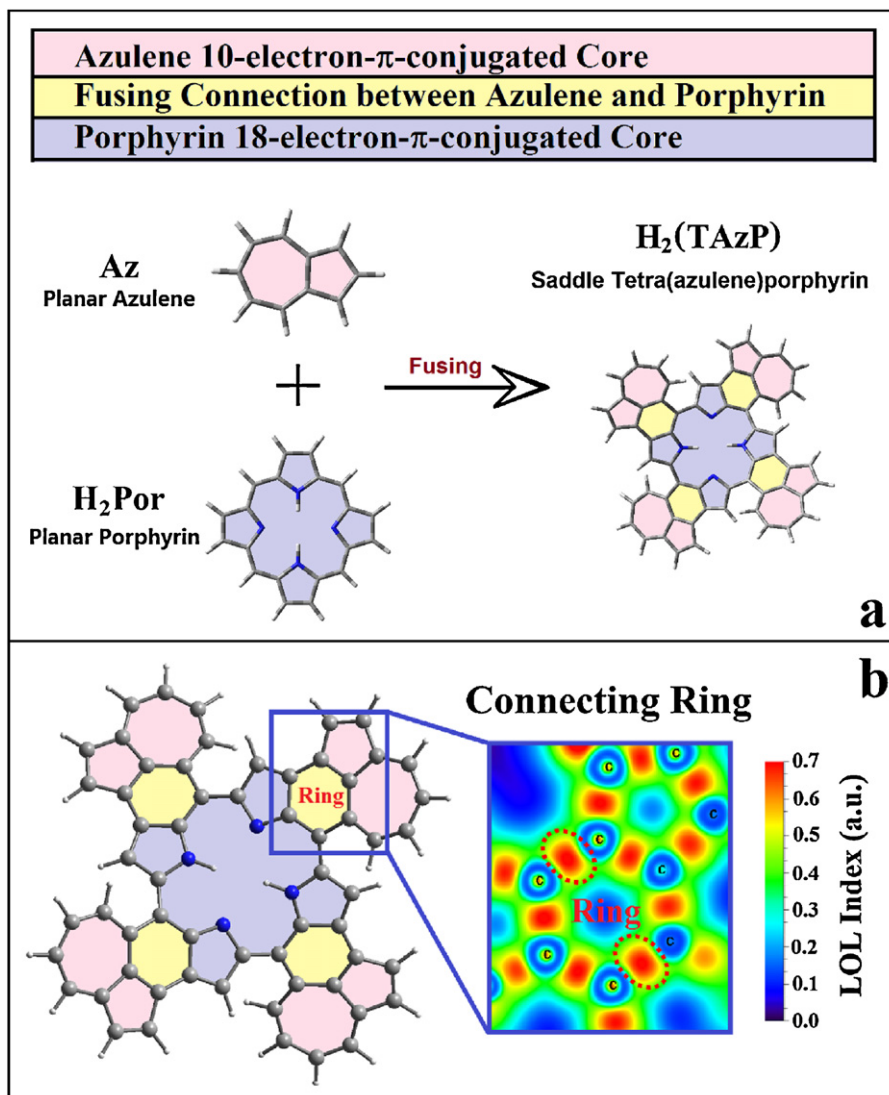

Fig. 1. Uniform TAzP conjugated skeleton. (a) Conjugated model of TAzP skeleton. (b) Localized orbital locator (LOL) analysis for all occupied π orbitals of $H_2(TAzP)$.
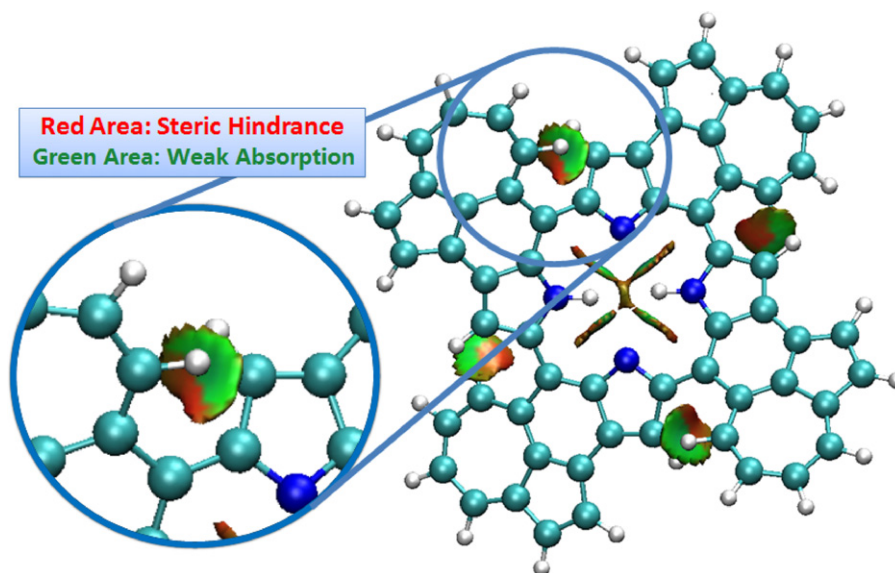
Fig. 2. Reduced density gradient (RDG) model for $H_2(TAzP)$.
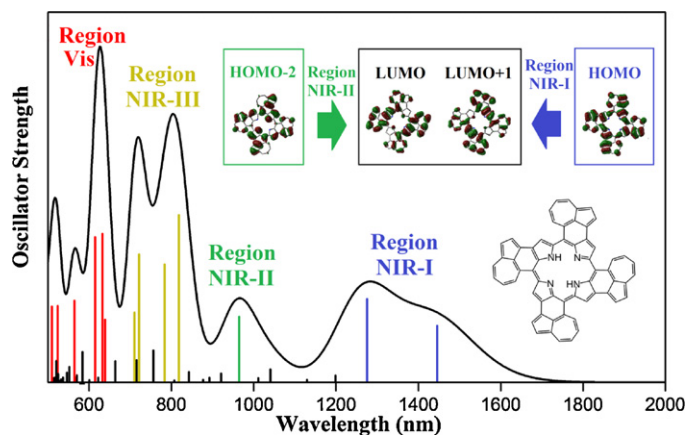

Fig. 3. Simulated UV–Vis–NIR spectrum and main electron transition models for $H_2(TAzP)$ (blue: Region NIR-I; green: Region NIR-II; yellow: Region NIR-III; red: Region Vis). (For interpretation of the references to color in this figure legend, the reader is referred to the web version of this article.)

3.2. Nature of the broad near-IR electronic absorption of $H_2(TAzP)$

Fig. 3 shows the simulated electronic absorption spectrum of $H_2(TAzP)$, which can be divided into four regions due to the different electron transition models, Fig. 3 and Table S2 (Supporting Information).

In Region NIR-I, an astonishingly red-shifted NIR absorption band from 1050 to 1450 nm was revealed, which corresponds well with the experimentally observed one [29,30]. Absorptions in this region is mainly due to the electron transitions of HOMO → LUMO/LUMO+1, which are assigned to the Q bands of $H_2(TAzP)$ [92–95]. According to TDDFT, the Q bands are assigned as:

$$\Phi_{^1B \leftarrow ^1A}^{1446\,nm} \approx 0.639\Psi_{H(a)}^{L(b)} - 0.253\Psi_{H-2(a)}^{L(b)} - 0.126\Psi_{H(a)}^{L+1(b)}$$
$$- 0.118\Psi_{H-2(a)}^{L+1(b)} - 0.107\Psi_{L(b)}^{H(a)};$$

$$\Phi_{^1B \leftarrow ^1A}^{1275\,nm} \approx 0.658\Psi_{H(a)}^{L+1(b)} - 0.178\Psi_{H-4(a)}^{L(b)} - 0.135\Psi_{H-4(a)}^{L+1(b)}$$
$$- 0.118\Psi_{H-2(a)}^{L+1(b)} + 0.112\Psi_{H(a)}^{L(b)}.$$

It is noteworthy that the excited states with $|c_{m \to n}| < 0.1$ are ignored in the TD-DFT transition equations since the electron transition model of MO(m) → MO(n) does not have obvious effect on the TD-DFT result when $c_{m \to n}^2 / \sum c_{m \to n}^2 < 0.02$. As shown in Fig. S2 (Supporting Information), the LUMO/LUMO+1 energy is −3.74/−3.63 eV for $H_2(TAnP)$, while the HOMO energy is as high as −4.35 eV, resulting in the very narrow gap between HOMO and LUMO/LUMO+1 of 0.61/0.72 eV and the exciting energy of 0.86/0.97 eV for the transition between S_0 and S_1/S_2. The HOMO–LUMO/LUMO+1 gaps for $H_2(TAzP)$ are much lower in comparison with other tetrapyrrole counterparts such as 2.93 and 2.91 eV for porphyrin, 2.73 and 2.63 eV for tetraazaporphyrin, 2.19 and 2.15 eV for phthalocyanine, 1.92 and 1.78 eV for napthalocyanine, and 0.86 and 0.96 eV for anthracocyanine [23,25,98]. This clearly explains the significantly red-shifted nature of these bands of $H_2(TAzP)$s in comparison with those for other tetrapyrrole compounds.

An intense NIR absorption band observed from 900 to 1050 nm is named as Region NIR-II, which also corresponds well with the experimental findings [29,30]. This band is mainly attributed to the electronic transitions of HOMO−2 → LUMO/LUMO+1 and assigned to the Soret bands of $H_2(TAzP)$ [92–95]. According to TDDFT, the Soret band of $H_2(TAnP)$ is assigned as:

$$\Phi_{^1B \leftarrow ^1A}^{964\,nm} \approx 0.516\Psi_{H-2(a)}^{L+1(b)} + 0.291\Psi_{H-2(a)}^{L(b)} + 0.251\Psi_{H-4(a)}^{L(b)}$$
$$+ 0.203\Psi_{H-4(a)}^{L+1(b)} + 0.184\Psi_{H(a)}^{L(b)}.$$

As shown in Fig. S2 (Supporting Information), the gaps between HOMO−2 and LUMO/LUMO+1 are still only 1.02/1.19 eV for $H_2(TAzP)$, leading to the significantly decreased Soret excited energy of 1.29 eV for $H_2(TAzP)$. The result indicates the significant influence of the peripheral π_{10e}^{Az} units on the electronic structure of the central π_{18e}^{Por} core.

In addition, a new absorption band was found in the region of 700–900 nm, Region NIR-III. This band is mainly attributed to the electronic transitions of HOMO−3/HOMO−4 → LUMO/LUMO+1/LUMO+2 and HOMO → LUMO+4/LUMO+5. In other word, this absorption band originates mainly from two types of electron transitions: one from semi-core-level occupied orbitals to frontier virtual orbitals, and another from frontier occupied orbitals to shell-level virtual orbitals. As

shown in Fig. S2 (Supporting Information), HOMO−3, LUMO+4, LUMO+4, and LUMO+5 mainly locate on the fused azulene units, while HOMO−4, LUMO, LUMO+1, and LUMO+2 are the coupling orbitals between azulene units and porphyrin core, indicating the origination of the new absorption band associated with the introduction of the peripheral conjugated systems. In addition, due to the significant red-shift of the Q/Soret bands of the TAzP skeleton, the absorption region between 700 and 900 nm in the electronic absorption spectrum of H_2(TAzP) is occupied by this new type of transition between the peripheral azulene units and central porphyrin core. According to TDDFT, the absorption band of H_2(TAnP) in Region NIR-III is assigned as:

$$\Phi_{^1B \leftarrow ^1A}^{818\,nm} \approx 0.523\Psi_{H-4(a)}^{L(b)} - 0.241\Psi_{H-2(a)}^{L(b)} - 0.219\Psi_{H-3(b)}^{L+2(a)}$$
$$- 0.188\Psi_{H(a)}^{L+5(b)} + 0.152\Psi_{H-1(a)}^{L+2(a)} + 0.122\Psi_{H(a)}^{L+1(b)}$$
$$- 0.120\Psi_{H(a)}^{L(b)} + 0.113\Psi_{H-5(a)}^{L+1(b)};$$

$$\Phi_{^1B \leftarrow ^1A}^{783\,nm} \approx 0.486\Psi_{H-3(b)}^{L+2(a)} + 0.360\Psi_{H-4(a)}^{L+1(b)} + 0.170\Psi_{H(a)}^{L+4(b)}$$
$$- 0.165\Psi_{H-2(a)}^{L(b)} - 0.144\Psi_{H(a)}^{L+5(b)} - 0.132\Psi_{H(a)}^{L(b)}$$
$$+ 0.131\Psi_{H-1(b)}^{L+2(a)};$$

$$\Phi_{^1B \leftarrow ^1A}^{721\,nm} \approx 0.404\Psi_{H(a)}^{L+4(b)} + 0.373\Psi_{H-5(a)}^{L(b)} - 0.328\Psi_{H-4(a)}^{L+1(b)}$$
$$+ 0.171\Psi_{H-3(b)}^{L+2(a)} + 0.112\Psi_{H(a)}^{L+1(b)} - 0.110\Psi_{H(a)}^{L+5(b)};$$

$$\Phi_{^1B \leftarrow ^1A}^{710\,nm} \approx 0.627\Psi_{H(a)}^{L+4(b)} + 0.152\Psi_{H-5(a)}^{L+1(b)}$$
$$- 0.128\Psi_{H-1(b)}^{L+3(a)} + 0.127\Psi_{H-4(a)}^{L(b)}.$$

Briefly summarizing above, the intense broad NIR absorption of H_2(TAzP) in Region NIR is actually formed by coupling of absorptions associated with various $\pi \to \pi^*$ electron transition types: the significantly red-shifted Q/Soret bands of H_2(TAzP) are in the region of 900–1450 nm, and a new absorption band related with the azulene units appears in the region of 700–900 nm (where the naphthalocyanine Q bands also appear in the same region). It is worth noting that electron transitions, which contribute to the absorption bands in Region NIR, result in the electron density moving between x and y axis for Q band, between azulene units and porphyrin core for Soret band, and between the azulene seven-membered rings and the combination of the porphyrin core and azulene five-membered rings for the new absorption band.

It is worth noting that for the purpose of explaining the experimental spectrum, Nakai and co-workers calculated the absorption spectrum of Ni(TAzP) at the level of [96]. Associated with the usually overestimated transition energies for the large conjugated systems of the B3LYP/6-31G(d) level, the Q/Soret bands take obvious red-shift in the simulated spectrum. As a consequence, the BP86 method was employed in the present case, resulting in better agreement with the experimental data as detailed below and in the Supporting Information.

3.3. Nature of the visible electronic absorption of H_2(TAzP)

For the bands in Region Vis (from 500 to 700 nm), the most intense absorptions appear at 632 nm and 615 nm, which are mainly attributed to the electron transitions of HOMO−5 → LUMO/LUMO+1 coupled with HOMO−1 → LUMO+3. As displayed in Fig. S2 (Supporting Information), the main electron-donating orbital HOMO−5 locates mainly on the central π_{18e}^{Por} core, while the main electron-accepting orbitals LUMO/LUMO+1 extensively locate at the total π_{58e}^{TAzP} conjugated system. Furthermore, the secondary important electron-donating orbital HOMO−1 and the secondary important electron-accepting orbital LUMO+3 locate on the peripheral π_{10e}^{Az} core. These results indicate that this band originates from the introduction of the peripherally-fused conjugated systems. According to TD-DFT theory, this new band is assigned as:

$$\Phi_{^1B \leftarrow ^1A}^{632\,nm} \approx 0.365\Psi_{H-5(a)}^{L(b)} - 0.362\Psi_{H-1(b)}^{L+3(a)} - 0.324\Psi_{H-5(a)}^{L+1(b)}$$
$$+ 0.221\Psi_{H-4(a)}^{L+1(b)} - 0.135\Psi_{H-2(a)}^{L+5(b)} - 0.109\Psi_{H-3(b)}^{L+2(a)}$$
$$- 0.108\Psi_{H-1(b)}^{L+6(a)};$$

$$\Phi_{^1B \leftarrow ^1A}^{615\,nm} \approx 0.546\Psi_{H-5(a)}^{L+1(b)} - 0.211\Psi_{H-1(b)}^{L+3(a)} - 0.208\Psi_{H-2(a)}^{L+4(b)}$$
$$+ 0.189\Psi_{H-5(a)}^{L(b)} - 0.122\Psi_{H-4(a)}^{L(b)} - 0.110\Psi_{H(a)}^{L+5(b)}$$
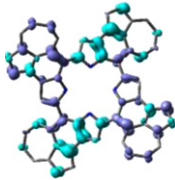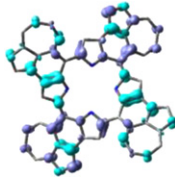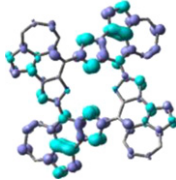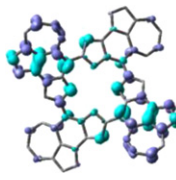$$- 0.106\Psi_{H(a)}^{L+1(b)}.$$
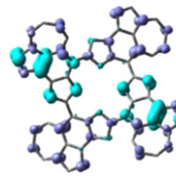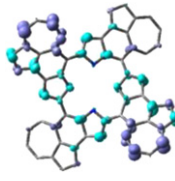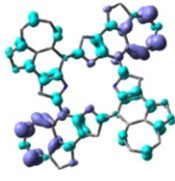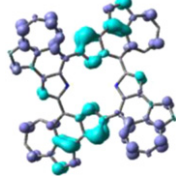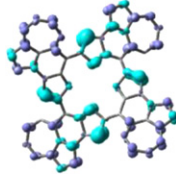
The maps of electron difference between the ground state and exited states are shown in Table 1. Obviously, the electronic absorption bands in Region Vis are due to the electron density transitions from the central π_{18e}^{Por} core to the peripheral π_{10}^{Az} units, respectively. As a total result, the Vis absorption bands of H_2(TAzP) actually originate from various types of $\pi \to \pi^*$ electron transitions among the frontier molecular orbitals.

3.4. Dependence of absorption spectrum on the peripheral electron-donating and electron-withdrawing substituents

To reveal the effect of the electron-donating groups attached at the periphery of the H_2(TAnP) macrocycle skeleton on the NIR electronic absorption spectra of tetraanthrac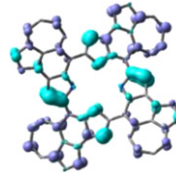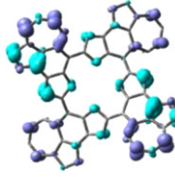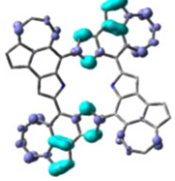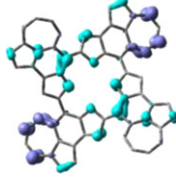enylporphyrin derivatives, $H_2[\alpha\text{-}(NH_2)_4TAzP]$, $H_2[\beta\text{-}(NH_2)_4TAzP]$, $H_2[\gamma\text{-}(NH_2)_4TAzP]$, $H_2[\delta\text{-}(NH_2)_4TAzP]$, $H_2[\varepsilon\text{-}(NH_2)_4TAzP]$, and $H_2[\zeta\text{-}(NH_2)_4TAzP]$ were calculated at the same TD-BP86/6-311+G(d,p)//B3LYP/6-311+G(d,p) level [97]. As exhibited in Fig. 4 and Fig. S3 (Supporting Information), the NIR absorption bands of $H_2[\alpha\text{-}(NH_2)_4TAzP]$ and $H_2[\varepsilon\text{-}(NH_2)_4TAzP]$ are significantly red-shifted due to the introduction of four strongly electron-donating NH_2 groups onto the periphery of TAzP macrocycle at the α/ε positions. However, the Q bands of $H_2[\beta\text{-}(NH_2)_4TAzP]$, $H_2[\gamma\text{-}(NH_2)_4TAzP]$, $H_2[\delta\text{-}(NH_2)_4TAzP]$, and $H_2[\zeta\text{-}(NH_2)_4TAzP]$ remain almost unshifted, indicating the slight substituent effect at the $\beta/\gamma/\delta/\zeta$ positions. According to our calculation results, the frontier orbital energies are significantly affected by incorporating peripheral NH_2 groups, which appears to form the microscopic mechanism of the above-mentioned red-shifted NIR absorption bands. The HOMO–LUMO-gap decreases from 0.61 eV for H_2(TAzP) to 0.39/0.46 eV for $H_2[\alpha\text{-}(NH_2)_4TAzP]/H_2[\varepsilon\text{-}(NH_2)_4TAzP]$, leading to the red-shifted NIR absorption bands to 1500–2500 nm, Fig. 5.

This is also true for $H_2(\alpha\text{-}F_4TAzP)$, $H_2(\beta\text{-}F_4TAzP)$, $H_2(\gamma\text{-}F_4TAzP)$, $H_2(\delta\text{-}F_4TAzP)$, $H_2(\varepsilon\text{-}F_4TAzP)$, and $H_2(\zeta\text{-}F_4TAzP)$ incorporating the peripheral electron-withdrawing F atoms [97]. As shown in Fig. 4 and Fig. S3 (Supporting Information), the NIR absorption bands of $H_2(\alpha\text{-}F_4TAzP)/H_2(\varepsilon\text{-}F_4TAzP)$ are red-shifted due to the introduction of four intense electron-withdrawing F atoms onto the periphery of TAzP ring at the α/ε positions, which is the direct result of the decreased HOMO–LUMO-gap of 0.56/0.53 eV for $H_2(\alpha\text{-}F_4TAzP)/H_2(\varepsilon\text{-}F_4TAzP)$, Fig. 5. Nevertheless, the substituent effect

Table 1
Electron density difference plots of electron transitions of H_2(TAzP).[a]

Region NIR-I	Region NIR-I	Region NIR-II	Region NIR-III	Region NIR-III
1446 nm (0.86 eV)	1275 nm (0.97 eV)	964 nm (1.29 eV)	818 nm (1.52 eV)	783 nm (1.58 eV)
f = 0.065	f = 0.096	f = 0.076	f = 0.193	f = 0.136
LHE = 14%	LHE = 20%	LHE = 16%	LHE = 36%	LHE = 27%
H → L (82%)	H → L+1 (87%)	H−2 → L+1 (53%)	H−4 → L (55%)	H−3 → L+2 (47%)
H−2 → L (13%)	H−4 → L (6%)	H−2 → L (17%)	H−2 → L (12%)	H−4 → L+1 (26%)
		H−4 → L (13%)	H−3 → L+2 (10%)	H → L+4 (6%)
		H−4 → L+1 (8%)	H → L+5 (7%)	H−2 → L (5%)
		H → L (7%)		

Region NIR-III	Region NIR-III	Region Vis	Region Vis	Region Vis
721 nm (1.72 eV)	710 nm (1.75 eV)	639 nm (1.94 eV)	632 nm (1.96 eV)	615 nm (2.02 eV)
f = 0.148	f = 0.081	f = 0.072	f = 0.172	f = 0.168
LHE = 29%	LHE = 17%	LHE = 15%	LHE = 33%	LHE = 32%
H → L+4 (33%)	H → L+5 (79%)	H−1 → L+3 (55%)	H−5 → L (27%)	H−5 → L+1 (60%)
H−5 → L (28%)		H−5 → L (28%)	H−1 → L+3 (26%)	H−1 → L+3 (9%)
H−4 → L+1 (21%)			H−5 → L+1 (21%)	H−2 → L+4 (9%)
H−3 → L+2 (6%)			H−4 → L+1 (10%)	H−5 → L (7%)

Region Vis	Region Vis	Region Vis		
564 nm (2.20 eV)	524 nm (2.37 eV)	510 nm (2.43 eV)		
f = 0.094	f = 0.088	f = 0.088		
LHE = 19%	LHE = 18%	LHE = 18%		
H−3 → L+3 (60%)	H−7 → L+1 (34%)	H−4 → L+5 (44%)		
H−2 → L+4 (22%)	H−1 → L+6 (30%)	H−6 → L+2 (15%)		
	H−2 → L+5 (15%)	H−7 → L+1 (13%)		
	H−4 → L+4 (5%)	H−1 → L+6 (7%)		

[a] Electron density transfers from the green area to the blue area. Excited states with less than 20,000 cm^{-1} and configurations which contribute more than 5% are shown.

of incorporating the electron-withdrawing groups is revealed to be much slighter than incorporating the electron-donating groups, Fig. 4.

As a consequence, the HOMO–LUMO gap changes significantly along with introducing electron-withdrawing and in particular electron-donating substituents at the α/δ positions, leading to the regulation of NIR absorption by the positions of peripheral substituents. In the case that the Gaussian band model with the half-bandwidth of 500 cm^{-1} is employed to simulate the real absorption, the NIR absorption band for $H_2[\alpha\text{-}(NH_2)_4TAzP]$ and $H_2[\varepsilon\text{-}(NH_2)_4TAzP]$ will cover the region of 1500–2500 nm, which are obviously different from the H_2(TAzP) NIR absorption band in the range of 1050–1450 nm, revealing that introduction of electron-donating groups onto different positions of the TAzP skeleton periphery is an effective way to generate novel near-IR (NIR) dyes with potential applications in different fields such as organic solar antenna collectors and solar cells [31–34].

3.5. Rule for designing the panchromatic tetrapyrrole organic functional molecules

Combination of the present result with previous investigations [22–30,58–65,99–101], the following points appear to be useful in the design of general panchromatic tetrapyrrole organic functional molecules, Scheme 2.

(1) *Low molecular symmetry*: It is well known that the high molecular symmetry generally leads to the high-order symmetrical electronic states, which in turn results in a number of transitions forbidden. As a result, reducing the molecular symmetry is an effective way to achieve full solar spectrum absorption due to the decrease in forbidden transition number. In terms of detailed experimental synthesis, introduction of large peripheral substituents which is able to induce distortion in the tetrapyrrole skeleton plays such kind of role [99–101].
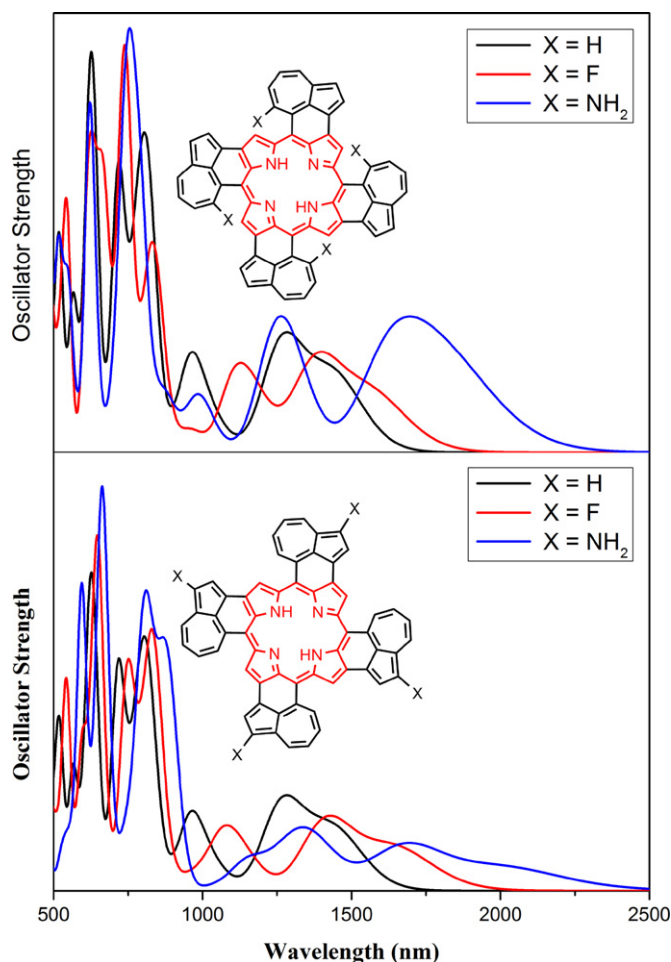
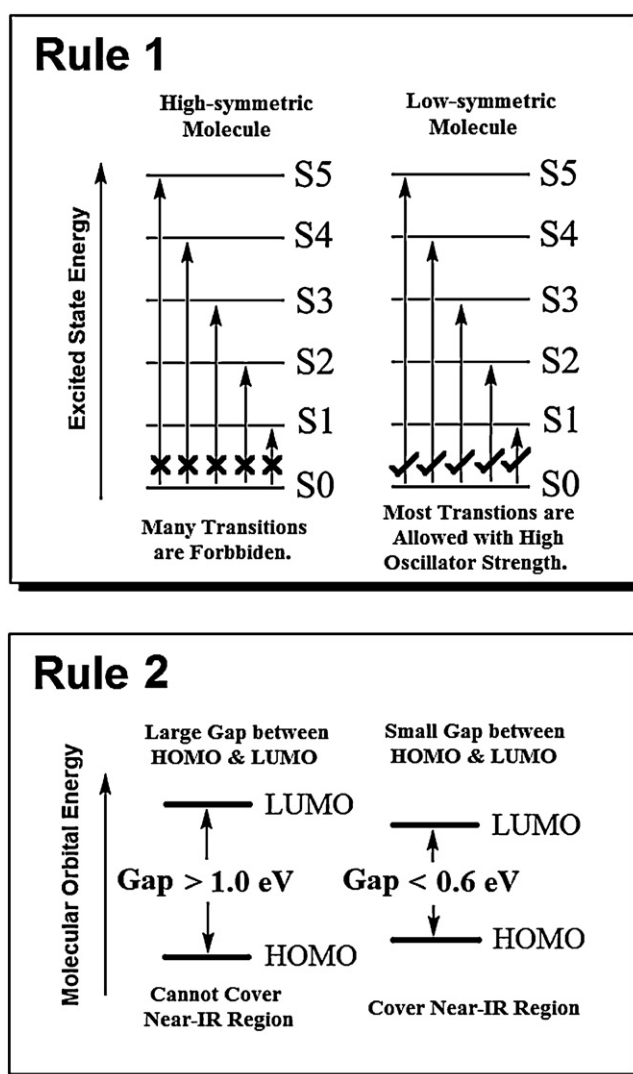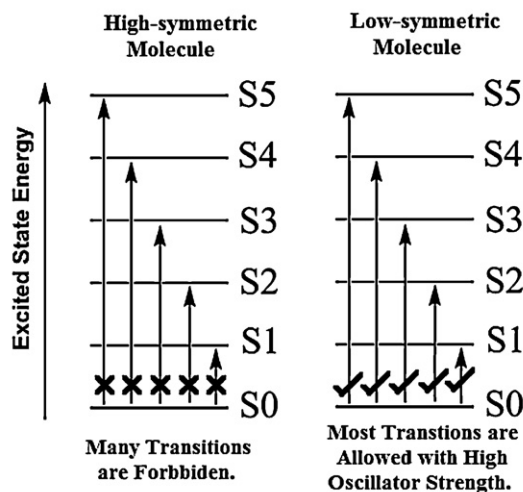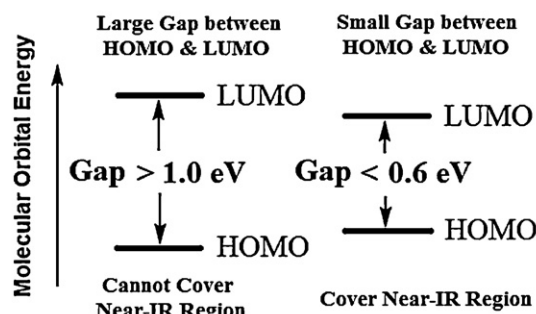**Fig. 4.** Simulated UV–Vis–NIR spectrum for $H_2(TAzP)$ and its derivatives with peripheral electron-donating/-withdrawing groups at α/ε position.

Scheme 2. Basic designing rules for panchromatic organic functional molecules.

Fig. 5. Frontier orbitals for $H_2(TAzP)$ and its derivatives with peripheral electron-donating/-withdrawing groups.

(2) *Narrow gap between HOMO and LUMO/LUMO+1*: Since the Q band of tetrapyrrole derivatives is mainly contributed by the electron transition between HOMO and LUMO/LUMO+1. If the gap between LUMO and HOMO/HOMO+1 decreases to 0.6 eV or lower, the Q band absorption will extend to the region beyond 2000 nm, leading to the broad absorption covering the full NIR region. To realize this aim, introducing fused peripheral conjugated substituents which are able to result in the frontier orbital coupling between peripheral conjugated units and central tetrapyrrole core seem to be an effective pathway [26]. In addition, incorporating electron-donating/withdrawing substituents onto the periphery of tetrapyrrole macrocycle, which can lead to the further change of frontier orbital energies, appears to be also meaningful.

4. Conclusion

The nature of the broad and intense NIR absorptions of $H_2(TAzP)$ derivatives is revealed on the basis of DFT and TD-DFT calculations, and the electron density moving direction between peripherally-fused ten electron-π-conjugated systems and the eighteen electron-π-conjugated core due to different types of electron transitions (actually associated with different absorption bands) has also been clarified. Theoretical calculation results

indicate that the astonishing narrow HOMO–LUMO-gap is responsible for the significant red-shift of the Q bands of TAzPs. A new absorption band appearing between 700 and 850 nm of TAzPs is considered as the result of electron density transfer from the eighteen electron-π-conjugated porphyrin core to the peripherally-fused azulene moieties. Introduction of electron-donating groups onto the periphery of azulene moiety, in particular at the α/ε positions, leads to novel NIR dyes with regulated red-shifted NIR absorption bands covering the full solar spectrum. Low molecular symmetry and narrow gap between HOMO and LUMO/LUMO+1 should be considered as necessary points in the molecular design of tetrapyrrole-based panchromatic organic functional molecules with potential applications in the fields of organic solar antenna collectors and organic solar cells.

Acknowledgements

Appendix A. Supplementary data

Supplementary data associated with this article can be found, in the online version, at http://dx.doi.org/10.1016/j.jmgm.2012.06.001.

References

[1] A. Tsuda, A. Osuka, Fully conjugated porphyrin tapes with electronic absorption bands that reach into infrared, Science 293 (2001) 79–82.
[2] Y. Nakamura, N. Aratani, H. Shinokubo, A. Takagi, T. Kawai, T. Matsumoto, Z.S. Yoon, D.Y. Kim, T.K. Ahn, D. Kim, A. Muranaka, N. Kobayashi, A. Osuka, A directly fused tetrameric porphyrin sheet and its anomalous electronic properties that arise from the planar cyclooctatetraene core, Journal of the American Chemical Society 128 (2006) 4119–4127.
[3] H.S. Cho, D.H. Jeong, S. Cho, D. Kim, Y. Matsuzaki, K. Tanaka, A. Tsuda, A. Osuka, Photophysical properties of porphyrin tapes, Journal of the American Chemical Society 124 (2002) 14642–14654.
[4] J. Jiang, M. Bao, L. Rintoul, D.P. Arnold, Vibrational spectroscopy of phthalocyanine and naphthalocyanine in sandwich-type (na)phthalocyaninato and porphyrinato rare earth complexes, Coordination Chemistry Reviews 250 (2006) 424–448.
[5] P. Peumans, A. Yakimov, S.R. Forrest, Small molecular weight organic thin-film photodetectors and solar cells, Journal of Applied Physics 93 (2003) 3693–3723.
[6] M. Hiramoto, H. Fujiwara, M. Yokoyama, p–i–n like behavior in three-layered organic solar cells having a co-deposited interlayer of pigments, Journal of Applied Physics 72 (1992) 3781–3787.
[7] X. Li, H. Wang, H. Wu, Phthalocyanines and their analogs applied in dye-sensitized solar cell, Structure and Bonding 135 (2010) 229–274.
[8] M.R. Detty, S.L. Gibson, S.J. Wagner, Current clinical and preclinical photosensitizers for use in photodynamic therapy, Journal of Medicinal Chemistry 27 (2004) 3897–3915.
[9] W.-S. Kuo, C.-N. Chang, Y.-T. Chang, M.-H. Yang, Y.-H. Chien, S.-J. Chen, C.-S. Yeh, Gold nanorods in photodynamic therapy, as hyperthermia agents, and in near-infrared optical imaging, Angewandte Chemie International Edition 49 (2010) 2711–2715.
[10] E.B. Dickerson, E.C. Dreaden, X. Huang, I.H. El-Sayed, H. Chu, S. Pushpanketh, J.F. McDonald, M.A. El-Sayed, Gold nanorod assisted near-infrared plasmonic photothermal therapy (PPTT) of squamous cell carcinoma in mice, Cancer Letters 269 (2008) 57–66.
[11] S. Ozlem, E.U. Akkaya, Thinking outside the silicon box: molecular AND logic as an additional layer of selectivity in singlet oxygen generation for photodynamic therapy, Journal of the American Chemical Society 131 (2009) 48–49.
[12] J. Fabian, H. Nakazumi, M. Matsuoka, Near-infrared absorbing dyes, Chemical Reviews 92 (1992) 1197–1226.
[13] M. Matsuoka, Infrared Absorbing Dyes, Plenum Press, New York, USA, 1990.
[14] R. Weissleder, A clearer vision for in vivo imaging, Nature Biotechnology 19 (2001) 316–317.
[15] S.A. Hilderbranda, R. Weissledera, Near-infrared fluorescence: application to in vivo molecular imaging, Current Opinion in Chemical Biology 14 (2010) 71–79.
[16] A. Seemann, H.-J. Egelhaaf, C.J. Brabec, J.A. Hauch, Influence of oxygen on semi-transparent organic solar cells with gas permeable electrodes, Organic Electronics 10 (2009) 1424–1428.
[17] Z.R. Hong, R. Lessmann, B. Maennig, Q. Huang, K. Harada, M. Riede, K. Leo, Antenna effects and improved efficiency in multiple heterojunction photovoltaic cells based on pentacene, zinc phthalocyanine, and C_{60}, Journal of Applied Physics 106 (2009) 064511.
[18] D. Qi, L. Zhang, L. Zhao, X. Cai, J. Jiang, A special conjugated model around sp^3 carbon atoms: density functional theory study on the homoaromatic electron delocalization and applications of benzo-fused tetra(triptycene)porphyrins, ChemPhysChem: A European Journal of Chemical Physics and Physical Chemistry 13 (2012) 2046–2054.
[19] NASA's Goddard space flight center in Greenbelt, Md., NASA develops super-black material that absorbs light across multiple wavelength bands, http://www.nasa.gov/topics/technology/features/super-black-material_prt.htm
[20] E.E. Narimanov, H. Li, Y.A. Barnakov, T.U. Tumkur, M.A. Noginov, Darker than black: radiation-absorbing metamaterial arXiv:1109.5469v1.
[21] G. de la Torre, C.G. Claessen, T. Torres, Phthalocyanines: old dyes, new materials. Putting color in nanotechnology, Chemical Communications (2007) 2000–2015.
[22] B.D. Rihter, M.E. Kenney, W.E. Ford, M.A.J. Rodgers, Photochromic reactions involving palladium (II) octabutoxynaphthalocyanine and molecular oxygen, Journal of the American Chemical Society 115 (1993) 8146–8152.
[23] Y. Bian, J. Jiang, Y. Tao, M.T.M. Choi, R. Li, A.C.H. Ng, P. Zhu, N. Pan, X. Sun, D.P. Arnold, Z.-Y. Zhou, H.-W. Li, T.C.W. Mak, D.K.P. Ng, Tuning the valence of the cerium center in (na)phthalocyaninato and porphyrinato cerium double-deckers by changing the nature of the tetrapyrrole ligands, Journal of the American Chemical Society 125 (2003) 12257–12266.
[24] A. Muranaka, M. Yonehara, M. Uchiyama, Azulenocyanine: a new family of phthalocyanines with intense near-IR absorption, Journal of the American Chemical Society 132 (2010) 7844–7845.
[25] N.K.S. Davis, A.L. Thompson, H.L. Anderson, A porphyrin fused to four anthracenes, Journal of the American Chemical Society 133 (2011) 30–31.
[26] D. Qi, L. Zhang, Y. Zhang, Y. Bian, J. Jiang, Nature of the intense near-IR absorption and unusual broad UV–visible–NIR spectra of azulenocyanines: density functional theory studies, Journal of Physical Chemistry A 114 (2010) 13411–13417.
[27] D. Qi, J. Jiang, Toward panchromatic organic functional molecules: density functional theory study on the electronic absorption spectra of substituted tetraanthracenylporphyrins, Journal of Physical Chemistry A 115 (2011) 13811–13820.
[28] J.L. Sessler, A. Gebauer, S.J. Weghorn, Expanded porphyrins, The Porphyrin Handbook 2 (2000) 55–124.
[29] K. Kurotobi, K.S. Kim, S.B. Noh, D. Kim, A. Osuka, A quadruply azulene-fused porphyrin with intense near-IR absorption and a large two-photon absorption cross section, Angewandte Chemie International Edition 45 (2006) 3944–3947.
[30] M.O. Senge, M. Fazekas, E.G.A. Notaras, W.J. Blau, M. Zawadzka, O.B. Locos, E.M. Ni Mhuircheartaigh, Nonlinear optical properties of porphyrins, Advanced Materials 19 (2007) 2737–2774.
[31] H. Imahori, T. Umeyama, S. Ito, Large π-aromatic molecules as potential sensitizers for highly efficient dye-sensitized solar cells, Accounts of Chemical Research 42 (2009) 1809–1818.
[32] A. Hagfeldt, G. Boschloo, L. Sun, L. Kloo, H. Pettersson, Dye-sensitized solar cells, Chemical Reviews 110 (2010) 6595–6663.
[33] P.V. Kamat, K. Tvrdy, D.R. Baker, J.G. Radich, Beyond photovoltaics: semiconductor nanoarchitectures for liquid-junction solar cells, Chemical Reviews 110 (2010) 6664–6688.
[34] A.W. Hains, Z. Liang, M.A. Woodhouse, B.A. Gregg, Molecular semiconductors in organic photovoltaic cells, Chemical Reviews 110 (2010) 6689–6735.
[35] J. Alda, J.M. Rico-Garcia, J.M. Lopez-Alonso, G. Boreman, Optical antennas for nano-photonic applications, Nanotechnology 16 (2005) S230–S234.
[36] D.K. Kotter, S.D. Novack, W.D. Slafer, P.J. Pinhero, Theory and manufacturing processes of solar nanoantenna electromagnetic collectors, Journal of Solar Energy Engineering 132 (2010) 011014.
[37] T. Nozawa, Y. Arakawa, Detailed balance limit of the efficiency of multilevel intermediate band solar cells, Applied Physics Letters 98 (2011) 171108.
[38] P.G. Hoertz, A. Staniszewski, A. Marton, G.T. Higgins, C.D. Incarvito, A.L. Rheingold, G.J. Meyer, Toward exceeding the Shockley–Queisser limit: photoinduced interfacial charge transfer processes that store energy in excess of the equilibrated excited state, Journal of the American Chemical Society 128 (2006) 8234–8245.
[39] S. Mori, M. Nagata, Y. Nakahata, K. Yasuta, R. Goto, M. Kimura, M. Taya, Enhancement of incident photon-to-current conversion efficiency for phthalocyanine-sensitized solar cells by 3D molecular structuralization, Journal of the American Chemical Society 132 (2010) 4054–4055.
[40] N. López, L.A. Reichertz, K.M. Yu, K. Campman, W. Walukiewicz, Engineering the electronic band structure for multiband solar cells, Physical Review Letters 106 (2011) 028701.
[41] D.M. Kaschak, J.T. Lean, C.C. Waraksa, G.B. Saupe, H. Usami, T.E. Mallouk, Photoinduced energy and electron transfer reactions in lamellar

polyanion/polycation thin films: toward an inorganic "leaf", Journal of the American Chemical Society 121 (1999) 3435–3445.

[42] A.B.J. Parusel, T. Wondimagegn, A. Ghosh, Do nonplanar porphyrins have red-shifted electronic spectra? A DFT/SCI study and reinvestigation of a recent proposal, Journal of the American Chemical Society 122 (2000) 6371–6374.

[43] J. Mack, N. Kobayashi, Low symmetry phthalocyanines and their analogues, Chemical Reviews 111 (2011) 281–321.

[44] Y. Zhang, J. Jiang, Circular dichroism of chiral 1,8,15,22-tetra(alkoxyl)phthalocyaninato lead and yttrium complexes: time-dependent density functional theory calculations, Journal of Physical Chemistry A 113 (2009) 12179–12186.

[45] S.P. Keizer, J. Mack, B.A. Bench, S.M. Gorun, M.J. Stillman, Spectroscopy and electronic structure of electron deficient zinc phthalocyanines, Journal of the American Chemical Society 125 (2003) 7067–7085.

[46] N. Kobayashi, H. Miwa, V.N. Nemykin, Adjacent versus opposite type di-aromatic ring-fused phthalocyanine derivatives: synthesis, spectroscopy, electrochemistry, and molecular orbital calculations, Journal of the American Chemical Society 124 (2002) 8007–8020.

[47] M. Aoudia, G. Cheng, V.O. Kennedy, M.E. Kenney, M.A.J. Rodgers, Synthesis of a series of octabutoxy- and octabutoxybenzophthalocyanines and photo-physical properties of two members of the series, Journal of the American Chemical Society 119 (1997) 6029–6039.

[48] J. Andzelm, A.M. Rawlett, J.A. Orlicki, J.F. Snyder, Optical properties of phthalo-cyanine and naphthalocyanine compounds, Journal of Chemical Theory and Computation 3 (2007) 870–877.

[49] D.G. Hilmey, M. Abe, M.I. Nelen, C.E. Stilts, G.A. Baker, S.N. Baker, F.V. Bright, S.R. Davies, S.O. Gollnick, A.R. Oseroff, S.L. Gibson, R. Hilf, M.R. Detty, Water-soluble, core-modified porphyrins as novel, longer-wavelength-absorbing sensitizers for photodynamic therapy: II. Effects of core heteroatoms and meso-substituents on biological activity, Journal of Medicinal Chemistry 45 (2002) 449–461.

[50] T.K. Chandrashekar, S. Venkatraman, Core-modified expanded porphyrins: new generation organic materials, Accounts of Chemical Research 36 (2003) 676–691.

[51] Y. You, S.L. Gibson, R. Hilf, T.Y. Ohulchanskyya, M.R. Detty, Core-modified porphyrins. Part 4: Steric effects on photophysical and biological properties in vitro, Bioorganic and Medicinal Chemistry 13 (2005) 2235–2251.

[52] E.J. Ngen, T.S. Daniels, R.S. Murthy, M.R. Dettyb, Y. You, Core-modified por-phyrins. Part 6: Effects of lipophilicity and core structures on physicochemical and biological properties in vitro, Bioorganic and Medicinal Chemistry 16 (2008) 3171–3183.

[53] Y. You, S.L. Gibsonb, M.R. Detty, Core-modified porphyrins. Part 5: Electronic effects on photophysical and biological properties in vitro, Bioorganic and Medicinal Chemistry 13 (2005) 5968–5980.

[54] N. Sprutta, M. Siczek, L. Latos-Grazynski, L. Pawlicki, L. Szterenberg, T. Lis, Dioxadiazuliporphyrin: a near-IR redox switchable chromophore, Journal of Organic Chemistry 72 (2007) 9501–9509.

[55] T.D. Lash, D.A. Colby, S.R. Graham, S.T. Chaney, Synthesis, spectroscopy, and reactivity of meso-unsubstituted azuliporphyrins and their heteroanalogues, Oxidative ring contractions to carba-, oxacarba-, thiacarba-, and selenacarba-porphyrins, Journal of Organic Chemistry 69 (2004) 8851–8864.

[56] T.D. Lash, S.T. Chaney, D.T. Richter, Conjugated macrocycles related to the por-phyrins. 12.1 oxybenzi-and oxypyriporphyrins: aromaticity and conjugation in highly modified porphyrinoid structures, Journal of Organic Chemistry 63 (1998) 9076–9088.

[57] Y. Matano, T. Nakabuchi, S. Fujishige, H. Nakano, H. Imahori, Redox-coupled complexation of 23-phospha-21-thiaporphyrin with group 10 metals: a con-venient access to stable core-modified isophlorin–metal complexes, Journal of the American Chemical Society 130 (2008) 16446–16447.

[58] Y. Zhang, X. Cai, P. Yao, H. Xu, Y. Bian, J. Jiang, Location of the hole and acid proton in neutral nonprotonated and protonated mixed (phthalocyan-inato)(porphyrinato) yttrium double-decker complexes: density functional theory calculations, Chemistry – A European Journal 13 (2007) 9503–9514.

[59] J. Jiang, D.K.P. Ng, A decade journey in the chemistry of sandwich-type tetrapyrrolato-rare earth complexes, Accounts of Chemical Research 42 (2009) 79–88.

[60] J. Jiang, Y. Bian, F. Furuya, W. Liu, M.T.M. Choi, N. Kobayashi, H.-W. Li, Q. Yang, T.C.W. Mak, D.K.P. Ng, Synthesis, structure, spectroscopic proper-ties, and electrochemistry of rare earth sandwich compounds with mixed 2,3-naphthalocyaninato and octaethylporphyrinato ligands, Chemistry – A European Journal 7 (2001) 5059–5069.

[61] R. Wang, R. Li, Y. Bian, C.-F. Choi, D.K.P. Ng, J. Dou, D. Wang, P. Zhu, C. Ma, R.D. Hartnell, D.P. Arnold, J. Jiang, Studies of "pinwheel-like" bis[1,8,15,22-tetrakis(3-pentyloxy)-phthalocyaninato] rare earth(III) double-decker complexes, Chemistry – A European Journal 11 (2005) 7351–7357.

[62] Y. Bian, R. Wang, J. Jiang, C.-H. Lee, J. Wang, D.K.P. Ng, Synthesis, spec-troscopic characterisation and structure of the first chiral heteroleptic bis(phthalocyaninato) rare earth complexes, Chemical Communications (2003) 1194–1195.

[63] R. Wang, R. Li, Y. Li, X. Zhang, P. Zhu, P.-C. Lo, D.K.P. Ng, N. Pan, C. Ma, N. Kobayashi, J. Jiang, Controlling the nature of mixed (phthalocyani-nato)(porphyrinato) rare-earth(III) double-decker complexes: the effects of nonperipheral alkoxy substitution of the phthalocyanine ligand, Chemistry – A European Journal 12 (2006) 1475–1485.

[64] X. Zhang, A. Muranaka, W. Lv, Y. Zhang, Y. Bian, J. Jiang, N. Kobayashi, Opti-cally active mixed phthalocyaninato–porphyrinato rare-earth double-decker complexes: synthesis, spectroscopy, and solvent-dependent molecular con-formations, Chemistry – A European Journal 14 (2008) 4667–4674.

[65] Y. Bian, Y. Zhang, Z. Ou, J. Jiang, Chemistry of sandwich tetrapyrrole rare earth complexes, Handbook of Porphyrin Science 14 (2010) 249–460.

[66] A.D. Becke, Density-functional thermochemistry: III. The role of exact exchange, Journal of Chemical Physics 98 (1993) 5648–5652.

[67] C. Lee, W. Yang, R.G. Parr, Development of the colle-salvetti correlation-energy formula into a functional of the electron density, Physical Review B 37 (1988) 785–789.

[68] S. Yan, Y. Bu, Z. Cao, P. Li, Coupling character between imidazole and imidazole cation: implication for the coupling modes of biomolecular residues, Journal of Physical Chemistry A 108 (2004) 7038–7049.

[69] D. Qi, Y. Zhang, L. Zhang, J. Jiang, Nature of the intense absorption and unusual broad UV–vis–NIR spectra of azulencyanines: density functional theory study, Journal of Physical Chemistry A 114 (2010) 1931–1938.

[70] L. Wan, D. Qi, Y. Zhang, J. Jiang, Controlling the directionality of charge trans-fer in phthalocyaninato zinc sensitizer for a dye-sensitized solar cell: density functional theory studies, Physical Chemistry Chemical Physics 13 (2011) 1639–1648.

[71] D. Qi, L. Zhang, L. Wan, Y. Zhang, Y. Bian, J. Jiang, Conformational effects, molec-ular orbitals, and reaction activities of bis(phthalocyaninato) lanthanum double-deckers: density functional theory calculations, Physical Chemistry Chemical Physics 13 (2011) 13277–13286.

[72] L. Wan, D. Qi, Y. Zhang, The effect of β-saturated pyrrolic rings on the elec-tronic structures and aromaticity of magnesium porphyrin derivatives: a density functional study J, Journal of Molecular Graphics and Modelling 30 (2011) 15–23.

[73] V.N. Nemykin, R.G. Hadt, R.V. Belosludov, H. Mizuseki, Y. Kawazoe, Influence of molecular geometry, exchange-correlation functional, and solvent effects in the modeling of vertical excitation energies in phthalocyanines using time-dependent density functional theory (TDDFT) and polarized contin-uum model TDDFT methods: can modern computational chemistry methods explain experimental controversies? Journal of Physical Chemistry A 111 (2007) 12901–12913.

[74] S.U. Lee, J.C. Kim, H. Mizuseki, Y. Kawazoe, The origin of the halogen effect on the phthalocyanine green pigments, Chemistry – An Asian Journal 5 (2010) 1341–1346.

[75] G.A. Peralta, M. Seth, H. Zhekova, T. Ziegler, Magnetic circular dichroism of phthalocyanine (M = Mg, Zn) and tetraazaporphyrin (M = Mg, Zn, Ni) metal complexes. A computational study based on time-dependent density func-tional theory, Inorganic Chemistry 47 (2008) 4185–4198.

[76] M.P. Donzello, C. Ercolani, K.M. Kadish, G. Ricciardi, A. Rosa, P.A. Stuzhin, Tetrakis(thiadiazole)porphyrazines: 5. Electrochemical and DFT/TDDFT stud-ies of the free-base macrocycle and its Mg^{II}, Zn^{II}, and Cu^{II} complexes, Inorganic Chemistry 46 (2007) 4145–4157.

[77] L. Zhang, D. Qi, Y. Zhang, Y. Bian, J. Jiang, Density functional theory studies on the structures and electronic communication of meso-ferrocenylporphyrins: long range orbital coupling via porphyrin core, Journal of Molecular Graphics and Modelling 29 (2011) 717–725.

[78] A.D. Becke, Density-functional exchange-energy approximation with correct asymptotic behavior, Physical Review A 38 (1988) 3098–3100.

[79] J.P. Perdew, Density functional approximation for the correlation energy of the inhomogeneous electron gas, Physical Review B 33 (1986) 8822–8824.

[80] X. Cai, Y. Zhang, D. Qi, J. Jiang, Density functional theory study on the semiconducting properties of metal phthalocyanine compounds: effect of axially coordinated ligand, Journal of Physical Chemistry A 113 (2009) 2500–2506.

[81] Y. Zhang, X. Cai, Y. Zhou, X. Zhang, H. Xu, Z. Liu, X. Li, J. Jiang, Structures and spectroscopic properties of bis(phthalocyaninato) yttrium and lanthanum complexes: theoretical study based on density functional theory calculations, Journal of Physical Chemistry A 111 (2007) 392–400.

[82] Y. Zhang, X. Zhang, Z. Liu, Y. Bian, J. Jiang, Structures and properties of 1,8,15,22-tetrasubstituted phthalocyaninato-lead complexes: the substitu-tional effect study based on density functional theory calculations, Journal of Physical Chemistry A 109 (2005) 6363–6370.

[83] A. Zhong, Y. Bian, Y. Zhang, Semiconductor performance of phthalocyaninato lead complex and its nonperipheral substituted derivatives for organic field effect transistors: density functional theory calculations, Journal of Physical Chemistry C 114 (2010) 3248–3255.

[84] E.R. Johnson, S. Keinan, P. Mori-Sanchez, J. Contreras-Garcia, A.J. Cohen, W. Yang, Revealing noncovalent interactions, Journal of the American Chemical Society 132 (2010) 6498–6506.

[85] T. Lu, F. Chen, A multifunctional wavefunction analyzer, Journal of Computa-tional Chemistry 33 (2012) 580–592.

[86] T. Lu, Multiwfn, Revision 2. 1, University of Science and Technology Beijing, Beijing, China, 2011.

[87] A.D. Becke, K.E. Edgecombe, A simple measure of electron localization in atomic and molecular systems, Journal of Chemical Physics 92 (1990) 5397–5403.

[88] A. Savin, O. Jepsen, J. Flad, O.K. Andersen, H. Preuss, H.G. von Schnering, Electron localization in solid-state structures of the elements: the diamond structure, Angewandte Chemie International Edition 31 (1992) 187–188.

[89] V. Tsirelson, A. Stash, Determination of the electron localization function from electron density, Chemical Physics Letters 351 (2002) 142–148.

[90] H.L. Schmider, A.D. Becke, Chemical content of the kinetic energy density, Journal of Molecular Structure (THEOCHEM) 527 (2000) 51–61.

[91] M.J. Frisch, et al., Gaussian 03, Revision B. 05, Gaussian, Inc., Pittsburgh, PA, 2004.

[92] J. Mack, M.J. Stillman, Electronic structures of metal phthalocyanine and porphyrin complexes form analysis of the UV–vis absorption and magnetic circular dichroism spectra and molecular orbital calculations, The Porphyrin Handbook 16 (2003) 43–116.

[93] M.J. Stillman, Theoretical aspects of the optical spectroscopy of porphyrinoids, Handbook of Porphyrin Science 14 (2010) 461–524.

[94] J. Mack, Y. Asano, N. Kobayashi, M.J. Stillman, Application of MCD spectroscopy and TD-DFT to a highly non-planar porphyrinoid ring system. New insights on red-shifted porphyrinoid spectral bands, Journal of the American Chemical Society 127 (2005) 17697–17711.

[95] T. Fukuda, N. Kobayashi, UV–visible spectroscopic properties of phthalocyanines and related macrocycles, Handbook of Porphyrin Science 9 (2010) 1–650.

[96] K. Nakai, K. Kurotobi, A. Osuka, M. Uchiyama, N. Kobayashi, Electronic structures of azulene-fused porphyrins as seen by magnetic circular dichroism and TD-DFT calculations, Journal of Inorganic Biochemistry 102 (2008) 466–471.

[97] The reason we choose NH_2 and F as the representative of electron-donating and -withdrawing groups, respectively, includes the very extreme electronegativity of both NH_2 and F as well as the lack of p–π conjugation between TAzP skeleton and NH_2/F substituents, which renders both substituents to perform as "pure" electron-donating/-withdrawing groups.

[98] I. Lanzo, N. Russo, E. Sicilia, First-principle time-dependent study of magnesium-containing porphyrin-like compounds potentially useful for their application in photodynamic therapy, Journal of Physical Chemistry B 112 (2008) 4123–4130.

[99] S. Nakamura, S. Hiroto, H. Shinokubo, Synthesis and oxidation of cyclic tetraindole, Chemical Sciences 3 (2012) 524–527.

[100] N. Kobayashi, T. Furuyama, K. Satoh, Rationally designed phthalocyanines having their main absorption band beyond 1000 nm, Journal of the American Chemical Society 133 (2011) 19642–19645.

[101] R.P. Pandian, Y. Kim, P.M. Woodward, J.L. Zweier, P.T. Manoharanc, P. Kuppusamy, The open molecular framework of paramagnetic lithium octabutoxy-naphthalocyanine: implications for the detection of oxygen and nitric oxide using EPR spectroscopy, Journal of Materials Chemistry 16 (2006) 3609–3618.